J Physiol 591.12 (2013) pp 2987–2998

The Journal of Physiology

The voltage-dependent L-type Ca^{2+} ($Ca_V1.2$) channel C-terminus fragment is a bi-modal vasodilator

John P. Bannister[1], Marie Dennis Leo[1], Damodaran Narayanan[1], Wanchana Jangsangthong[1], Anitha Nair[1], Kirk W. Evanson[1], Judith Pachuau[1], Kyle S. Gabrick[2], Frederick A. Boop[2] and Jonathan H. Jaggar[1]

[1]*Departments of Physiology and* [2]*Neurosurgery, University of Tennessee Health Science Center, 894 Union Avenue, Suite 426, Memphis, TN 38163, USA*

Key points

- Voltage-dependent L-type Ca^{2+} ($Ca_V1.2$) channels are the major Ca^{2+} influx pathway and are central to contractility regulation in arterial smooth muscle cells.
- $Ca_V1.2$ exists as a full-length channel and undergoes cleavage to a short $Ca_V1.2$ and a C-terminus (CCt) fragment in rat and human arterial smooth muscle cells.
- CCt decreases $Ca_V1.2$ transcription and shifts the voltage dependence of current activation and inactivation to more depolarized potentials in arterial smooth muscle cells.
- CCt reduces pressure- and depolarization-induced vasoconstriction.
- CCt is a bi-modal vasodilator.

Abstract Voltage-dependent L-type Ca^{2+} channels ($Ca_V1.2$) are the primary Ca^{2+} entry pathway in vascular smooth muscle cells (myocytes). $Ca_V1.2$ channels control systemic blood pressure and organ blood flow and are pathologically altered in vascular diseases, which modifies vessel contractility. The $Ca_V1.2$ distal C-terminus is susceptible to proteolytic cleavage, which yields a truncated $Ca_V1.2$ subunit and a cleaved C-terminal fragment (CCt). Previous studies in cardiac myocytes and neurons have identified CCt as both a transcription factor and $Ca_V1.2$ channel inhibitor, with different signalling mechanisms proposed to underlie some of these effects. CCt existence and physiological functions in arterial myocytes are unclear, but important to study given the functional significance of $Ca_V1.2$ channels. Here, we show that CCt exists in myocytes of both rat and human resistance-size cerebral arteries, where it locates to both the nucleus and plasma membrane. Recombinant CCt expression in arterial myocytes inhibited $Ca_V1.2$ transcription and reduced $Ca_V1.2$ protein. CCt induced a depolarizing shift in the voltage dependence of both $Ca_V1.2$ current activation and inactivation, and reduced non-inactivating current in myocytes. Recombinant truncated CCt lacking a putative nuclear localization sequence (Δ92CCt) did not locate to the nucleus and had no effect on arterial $Ca_V1.2$ transcription or protein. However, Δ92CCt shifted the voltage dependence of $Ca_V1.2$ activation and inactivation similarly to CCt. CCt and Δ92CCt both inhibited pressure- and depolarization-induced vasoconstriction, although CCt was a far more effective vasodilator. These data demonstrate that endogenous CCt exists and reduces both $Ca_V1.2$ channel expression and voltage sensitivity in arterial myocytes. Thus, CCt is a bi-modal vasodilator.

(Received 22 January 2013; accepted after revision 4 April 2013; first published online 8 April 2013)

Corresponding author J. H. Jaggar: Department of Physiology, University of Tennessee Health Science Centre, 894 Union Avenue, Suite 426, Memphis, TN 38163, USA. Email: jjaggar@uthsc.edu

Abbreviations BSA, bovine serum albumin; $DCT^{-/-}$, distal C-terminus knockout; DMEM, Dulbecco's modified Eagle's medium; FBS, fetal bovine serum; GFP, green fluorescent protein; HEK, human embryonic kidney; NMDG, *N*-methyl-D-glucamine; Nimo, nimodipine; POPO-3, benzoxazolium, 2,2′- [1,3-propanediylbis[(dimethyliminio)-3, 1-propanediyl-1(4H)-pyridinyl-4-ylidene-1-propen-1-yl-3-ylidene]]bis[3-methyl]-, tetraiodide; PSS, physiological saline solution; WGA, wheat germ agglutinin

DOI: 10.1113/jphysiol.2013.251926

Introduction

Intracellular Ca^{2+} regulates a wide variety of cellular functions including contraction, cell proliferation, and transcription (Berridge, 1997; Jaggar *et al.* 2000). Voltage-dependent L-type Ca^{2+} channels ($Ca_V1.2$) are the primary Ca^{2+} entry pathway in vascular smooth muscle cells (Gollasch & Nelson, 1997). $Ca_V1.2$ channels regulate smooth muscle cell contractility and gene expression, which controls regional organ blood flow and systemic blood pressure (Gollasch & Nelson, 1997; Cartin *et al.* 2000; Jaggar *et al.* 2000; Amberg *et al.* 2004). Hypertension is associated with an elevation in arterial smooth muscle cell $Ca_V1.2$ channel protein and current density, leading to vasoconstriction (Sonkusare *et al.* 2006; Bannister *et al.* 2012). Pharmacological $Ca_V1.2$ channel blockers are one therapy used to alleviate clinical hypertension. Therefore, investigating molecular signals that control $Ca_V1.2$ channel functionality in arterial smooth muscle cells provides a better understanding of mechanisms that control vascular contractility.

$Ca_V1.2$ channels are composed of pore forming α_1, and auxiliary $\alpha_2\delta$ and β subunits (Catterall *et al.* 2005). In cardiac myocytes and neurons, the $Ca_V1.2$ intracellular C-terminus is susceptible to proteolytic cleavage, yielding a truncated (∼190 kDa, short) $Ca_V1.2$ subunit and a ∼50 kDa cleaved C-terminal fragment (CCt; De Jongh *et al.* 1991; Gomez-Ospina *et al.* 2006; Schroder *et al.* 2009). Recombinant short $Ca_V1.2$ channels generate larger whole-cell currents than do full length $Ca_V1.2$ subunits (Wei *et al.* 1994; Gerhardstein *et al.* 2000; Gao *et al.* 2000; Hulme *et al.* 2006). When expressed in tsA-201 cells, the CCt fragment re-associates with short $Ca_V1.2$ channels and shifts the voltage dependence of activation to more depolarized potentials (Hulme *et al.* 2006). In cardiac myocytes and neurons, the CCt fragment can also act as a transcription factor, although mechanisms described differ in these cell types (Gomez-Ospina *et al.* 2006; Schroder *et al.* 2009). Physiological functions of $Ca_V1.2$ truncation in arterial smooth muscle cells are unclear. Similarly unclear is whether CCt fragments are present and regulate $Ca_V1.2$ functionality in smooth muscle cells and arterial contractility. Given the importance of $Ca_V1.2$ channels in the vasculature, the focus of this study was to investigate the existence and physiological functions of CCt in smooth muscle cells of resistance-size arteries.

Here, we show for the first time that CCt is present in contractile smooth muscle cells of resistance-size arteries, where it locates to both the nucleus and plasma membrane. CCt decreases smooth muscle cell $Ca_V1.2$ subunit transcription and protein and shifts the voltage dependence of current activation and inactivation to more depolarized potentials. A truncated CCt (Δ92CCt) lacking the putative nuclear localization sequence did not alter $Ca_V1.2$ protein, but shifted $Ca_V1.2$ current voltage dependence similarly to CCt. CCt and Δ92CCt both reduced pressure- and depolarization-induced vasoconstriction, with CCt being a more effective vasodilator. In summary, we demonstrate that the CCt fragment reduces both $Ca_V1.2$ channel transcription and voltage sensitivity in smooth muscle cells and therefore, acts as a bi-modal vasodilator.

Methods

Ethical approval

Animal protocols used were reviewed and approved by the Animal Care and Use Committee at the University of Tennessee Health Science Centre. Human sample was obtained with institutional review board approval, written informed consent and in accordance with the guidelines of the *Declaration of Helsinki*.

Cell isolation and tissue preparation

Male Sprague Dawley rats (∼250 g) were killed by intraperitoneal injection of sodium pentobarbital (150 mg (kg body weight)$^{-1}$, Vortech Pharmaceuticals, Dearborn, MI, USA). The brain was removed and placed in chilled (4°C) physiological saline solution (PSS) containing (in mM): KCl 6, NaCl 112, $NaHCO_3$ 24, $MgSO_4$ 1.2, KH_2PO_4 1.2, $CaCl_2$ 1.8, and glucose 10. Middle cerebral, posterior cerebral, and cerebellar arteries (∼100–200 μm diameter) were removed for study. Where applicable, smooth muscle cells were dissociated from cerebral arteries using enzymes, as previously described (Jaggar, 2001). A human temporal lobe brain sample was obtained from a 16-year-old male who underwent a lobectomy for the treatment of epilepsy, but had no history of hypertension or stroke. Following excision, the brain sample was placed immediately into ice-cold (4°C) DMEM. Human cerebral arteries were dissected from the sample within 1–2 h of surgery and placed in ice-cold PSS.

CCt constructs

Full-length CCt, Δ92CCt, GFP tagged CCt (CCt-GFP) and GFP tagged Δ92CCt (Δ92CCt-GFP) constructs were produced by DNA Technologies Inc. (Gaithersburg, MD, USA) $Ca_V1.2e1b$ (Genbank accession number ABF85689.1) was used to generate the full-length CCt and Δ92CCt constructs. The region encompassing amino acids S1788–L2165 (377 amino acids) was inserted into pcDNA3.1 or pEGFP-N3 between *Bam*H1 and *Xho*1, to generate the full-length CCt and CCt-GFP constructs, respectively. The region encompassing amino acids S1880–L2165 (285 amino acids) was inserted into pcDNA3.1 or pEGFP-N3 between *Bam*H1 and *Xho*1,

to generate the Δ92CCt and Δ92CCt-GFP constructs, respectively. An ATG start codon was introduced proximal to the first amino acid codon in all constructs. The predicted molecular weights are ∼41 and ∼31 kDa for full-length CCt and Δ92CCt, respectively.

Cell culture and transfection

Human embryonic kidney (HEK)-293 cells were maintained at 37°C (21% O_2–5% CO_2) in DMEM (Cellgro, Manassas, VA, USA), supplemented with 10% FBS and 1% penicillin–streptomycin (Sigma-Aldrich, St Louis, MO, USA). HEK293 cells were transfected with pcDNA3.1 vector encoding full-length CCt (DNA Technologies Inc., Gaithersburg, MD, USA). Untransfected cells were used as a control.

Cerebral arteries were transfected using reverse permeabilization as previously described (Lesh *et al.* 1995). Arteries were transfected with either empty vector (pcDNA3.1, control) or pcDNA3.1 encoding CCt (DNA Technologies Inc., Gaithersburg, MD, USA) or Δ92CCt (GeneScript USA Inc., Piscatawny, NJ, USA). For confocal experiments arteries were transfected with pEGFP-N3 vectors encoding either CCt-GFP (DNA Technologies Inc., Gaithersburg, MD, USA) or Δ92CCt-GFP (GeneScript USA Inc., Piscatawny, NJ, USA). Arteries were maintained in culture (37°C, 21% O_2–5% CO_2) for 4 days in DMEM (Cellgro, Manassas, VA, USA) supplemented with 1% penicillin–streptomycin.

Protein analysis and biochemistry

Proteins were separated on either 12% (to visualize CCt fragments) or 7.5% (to resolve full length and truncated $Ca_V1.2$ protein) SDS–PAGE gels and analysed by Western Blotting. The 12% gels were initially probed with anti-CCt, then cut at the 75 kDa marker, stripped and re-probed for actin (below 75 kDa) and total $Ca_V1.2$ (above 75 kDa). The 7.5% gels were cut at the 75 kDa marker to allow simultaneous probing of blots for full length $Ca_V1.2$ with anti-CCt (upper portion) and actin (lower portion). Blots were then stripped and re-probed for total $Ca_V1.2$ (upper). Antibodies used were a custom anti-CCt raised to the distal $Ca_V1.2$ C-terminus (CDPGQDRAVVPEDES, Genemed Synthesis Inc., San Antonio, TX, USA), anti-$Ca_V1.2$ (Neuromab, Davis, CA, USA) and anti-actin (Millipore, Temecula, CA, USA).

Quantitative real-time PCR

Quantitative Taqman PCR reactions were carried out using an LC480 light cycler (Roche Applied Science, Indianapolis, IN, USA), as previously described (Bannister *et al.* 2012). Standard curves were run for all probe and primer pairs using four 10-fold dilutions of cDNA to determine PCR efficiency. $Ca_V1.2$ mRNA was calculated relative to the difference between fluorescence (Ct) values (ΔCt) for Rps5. Each reaction was performed in triplicate, with the mean used as a single experimental value. Gene specific primers and probes used were as previously described (Bannister *et al.* 2012).

Confocal imaging

Smooth muscle cells were plated onto poly-L-lysine-coated coverslips, fixed in 3.7% paraformaldehyde and permeabilized using 0.1% Triton X-100. Cells were blocked using 5% BSA and incubated in either wheat germ agglutinin (WGA; 1 mg ml^{-1}), anti-$Ca_V1.2$ antibody (1:100 dilution) or anti-CCt antibody (1:100 dilution) overnight at 4°C. Cells were washed in PBS and subsequently incubated with either anti-CCt antibody or POPO-3 (Life Technologies, Grand Island, NY, USA) nuclear stain (15 min, 4 mM), respectively. Cells incubated with WGA or anti-$Ca_V1.2$ antibody were washed with PBS and incubated with anti-mouse Alexa 546 secondary antibodies (1 h, 37°C). Cells incubated with anti-CCt antibody were incubated with anti-rabbit Alexa 488 (1 h, 37°C) secondary antibody. The specificity of the anti-CCt and Alexa 488 antibodies was confirmed by incubating smooth muscle cells with either boiled anti-CCt first followed by Alexa 488 antibodies or Alexa 488 antibody alone (Supplemental Figure S1). Coverslips were plated onto slides using a 1:1 glycerol:PBS mounting media and edges sealed.

Images were acquired using a laser-scanning confocal microscope (LSM5 Pascal, Carl Zeiss, Inc., Thornwood, NY, USA) and analysed using Zeiss LSM5 Pascal Colocalization Module software. Alexa 488 and GFP were excited at 488 nm and emission collected at 505–530 nm. Alexa 546 and POPO-3 were excited at 543 nm and emission collected at ≥560 nm. Isolated myocytes were imaged through the centre of the nucleus using a z-resolution of ∼1 μm and 512 × 512 pixel density. Laser intensity and detector gain were set below saturation and were maintained constant for each experiment. The average pixel intensity of regions that did not correspond to smooth muscle cells set the background value for each image. To calculate co-localization, a region of interest was drawn around each smooth muscle cell. Overlapping pixels from different fluorophores counted as co-localized and were expressed relative to the total number of pixels above background. Weighted co-localization was then calculated using the Zeiss LSM5 Pascal Colocalization Module software.

Patch-clamp electrophysiology

Smooth muscle cell voltage-dependent Ca^{2+} currents were recorded in isolated smooth muscle cells using the whole cell patch-clamp configuration using an Axopatch

200B amplifier (Axon Instruments, Sunnyvale, Ca, USA). Borosilicate glass electrodes (4–5 MΩ) were filled with pipette solution containing (in mM): $CsMeSO_4$ 135, CsCl 5, EGTA 5, MgATP 4, Na_2GTP 0.25, Hepes 10 and glucose 10 (pH 7.2 adjusted using CsOH). Extracellular bath solution contained (in mM): NMDG 130, $BaCl_2$ 20, $MgCl_2$ 1, Hepes 10 and glucose 10 (pH 7.4 adjusted using L-aspartic acid). Cell capacitance was measured by applying a 5 mV test pulse and correcting transients with series resistance compensation.

To measure whole-cell $Ca_V1.2$ currents, 300 ms pulses to between −60 and +60 mV were applied in 10 mV increments from a holding potential of –80 mV. Current–voltage (*I–V*) relationships were generated from the peak current obtained during 300 ms pulses. Inactivation was measured by applying 1 s conditioning pulses to between −80 and +60 mV in 10 mV increments prior to a 200 ms test pulse to 0 mV. Currents were filtered at 1 kHz, digitized at 5 kHz, and normalized to membrane capacitance. The rate of current inactivation was calculated from current decay during each 1 s conditioning pulse. Steady-state inactivation was calculated from the current generated during each 200 ms test pulse to 0 mV. To measure steady-state activation, tail currents were elicited by repolarization to −80 mV from 20 ms test pulses from −60 to +60 mV in 10 mV increments. Whole cell currents were filtered at 1 or 5 kHz and digitized at 5 or 20 kHz for the inactivation and activation protocols, respectively. P/–4 protocols were used to subtract leak and capacitive transients. Recorded traces were filtered using a low pass Bessel filter.

Steady-state inactivation and activation curves were fitted with a single power Boltzmann function:

$$I/I_{max} = R_{in} + (R_{max} - R_{in})/(1 + \exp((V - V_{\frac{1}{2}})/k)),$$

where I/I_{max} is the normalized peak current, V is the conditioning pre-pulse voltage, $V_{\frac{1}{2}}$ is the voltage for half-inactivation or half-activation, k is the slope factor, R_{in} is the proportion of non-inactivating current and R_{max} is the maximal current amplitude. Current inactivation was fitted with a single exponential function:

$$I_t = (A \times e^{(-t/\tau)}) + I_0,$$

where I_t is the inward current at time t, A the amplitude and I_0 the residual current.

Pressurized artery myography

Experiments were performed using control (empty vector) and either CCt or Δ92CCt-expressing arteries with PSS gassed with 21% O_2–5% CO_2–74% N_2 (pH 7.4). The endothelium was removed by passing an air bubble through the lumen of the vessel for ∼1 min followed by washing with PSS. Denuded arterial segments ∼2 mm in length were cannulated at each end in a perfusion chamber (Living Systems Instrumentation, St Albans, VT, USA) that was maintained at 37°C under constant PSS perfusion. Intravascular pressure was altered using an attached reservoir and monitored using a pressure transducer. Arterial diameter was measured (1 Hz) using a CCD camera mounted on a Nikon TS100-F microscope and automatic edge detection software (Ion Wizard software; Ionoptix, Milton, MA, USA) as previously described (Adebiyi *et al.* 2008). Myogenic tone was calculated as: $100 \times (1 - D_{active}/D_{passive})$, where D_{active} is the active arterial diameter and $D_{passive}$ the passive diameter determine by applying nimodipine (1 μM) and subsequent removal of extracellular Ca^{2+} by perfusing Ca^{2+}-free PSS supplemented with 5 mM EGTA. Endothelium denudation was confirmed by an absence of a response to the endothelial-dependent vasodilator carbachol (1 μM).

Statistical analysis

Summary data are presented as means ± SEM. Significance was determined using Student's unpaired *t* tests with the Welsh correction, or ANOVA followed by Student–Newman–Keuls for multiple groups. $P < 0.05$ was considered significant. Where applicable, power analysis was performed to verify that the sample size was sufficient to give a value of >0.8.

Results

The CCt fragment is present in both rat and human cerebral artery smooth muscle cells

A custom antibody was generated to an amino acid sequence located downstream of the cleavage site in the arterial smooth muscle cell $Ca_V1.2$ channel (Cheng *et al.* 2007). To determine the specificity of this antibody, CCt was expressed in HEK-293 cells. The predicted molecular weight of the cleaved CCt fragment is ∼41 kDa. The anti-CCt antibody detected a band consistent with this size in lysate from HEK cells transfected with CCt (Fig. 1*A*). This band was not present in the same protein lysates from control untransfected HEK-293 cells (Fig. 1*A*). A commercial $Ca_V1.2$ antibody that recognizes an amino acid sequence located in the intracellular DII to DIII linker was used to detect $Ca_V1.2$ proteins. This commercial antibody identified 190 and 240 kDa proteins consistent with short and full-length $Ca_V1.2$ channels, but did not detect the CCt fragment, in rat and human cerebral artery lysates (Fig. 1*B*). The anti-CCt antibody detected bands corresponding to both full-length $Ca_V1.2$ and the CCt fragment, but did not identify short $Ca_V1.2$, in rat and human cerebral arteries (Fig. 1*B* and

C). These data indicate that full length $Ca_V1.2$, short $Ca_V1.2$ and CCt are present in rat and human cerebral arteries.

Endogenous CCt locates to the plasma membrane and nucleus in arterial smooth muscle cells

Previous studies in cardiac myocytes and neurons have indicated that the CCt fragment translocates to the nucleus and acts as a nuclear transcription factor (Gomez-Ospina *et al.* 2006; Schroder *et al.* 2009). The intracellular distribution of the CCt fragment in arterial smooth muscle cells is unclear. To investigate endogenous CCt cellular distribution, smooth muscle cells were labelled with anti-CCt antibodies and either POPO-3, a nuclear label, or wheat germ agglutinin (WGA), a plasma membrane stain. Smooth muscle cells labelled with both boiled anti-CCt and Alexa 488 secondary antibodies or Alex 488 antibody alone did not emit fluorescence (Supplemental Figure S1). Confocal imaging indicated that the CCt antibody co-localized with POPO-3 (~26%) and WGA (~66%) when analysed using mean weighted pixel co-localization analysis (Fig. 2*A* and *B*). CCt has been shown to associate with short $Ca_V1.2$ channels (Hulme *et al.* 2006). To further investigate the plasma membrane localization of endogenous CCt, smooth muscle cells were labelled with anti-$Ca_V1.2$ antibody. $Ca_V1.2$ is present primarily (>95%) at the plasma membrane in arterial smooth muscle cells (Bannister *et al.* 2009, 2011, 2012). Anti-CCt and anti-$Ca_V1.2$ antibodies co-localized well (~70%), but not fully, suggesting that short $Ca_V1.2$

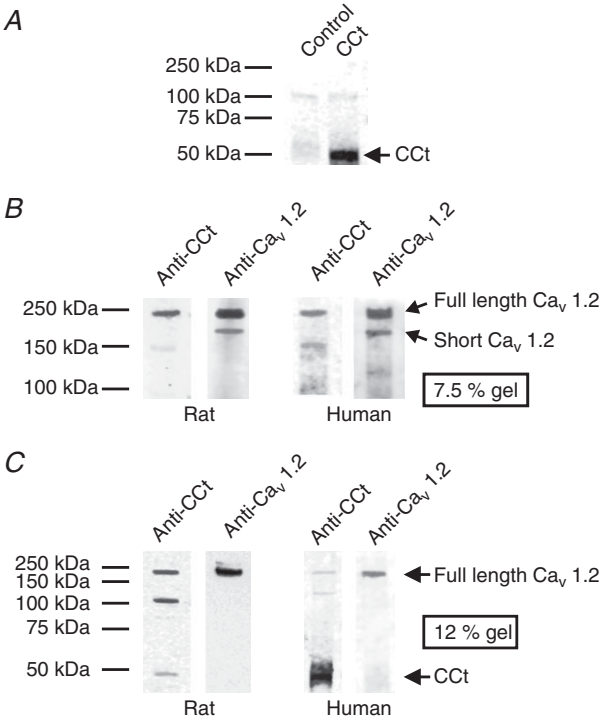

Figure 1. An antibody raised to the distal C-terminus of $Ca_V1.2$ detects cleaved CCt and full-length $Ca_V1.2$ subunit protein in rat and human cerebral arteries
A, representative Western blots illustrating detection of CCt fragment in lysates from HEK-293 cells overexpressing CCt. *B*, Western blots obtained from lysates separated on 7.5% Tris–glycine gels. Anti-CCt detected only full length $Ca_V1.2$. Anti-$Ca_V1.2$ detected both full length and truncated $Ca_V1.2$ subunit proteins. Blots are representative of 6 experiments for rat lysates. *C*, representative blots obtained from rat and human cerebral artery lysates separated on 12% Tris–glycine gels. Anti-CCt antibody detected full-length $Ca_V1.2$ and CCt fragment in rat and human cerebral arteries. Blots were stripped and re-probed with anti-$Ca_V1.2$ antibody to illustrate location of full-length $Ca_V1.2$ subunit protein. Blots are representative of 6 experiments for rat lysates. Human cerebral artery lysate used in *B* and *C* was obtained from a 16-year-old male patient with no history of hypertension or stroke. In each panel, brightness and contrast were equally adjusted to make regions of interest in images clearer.

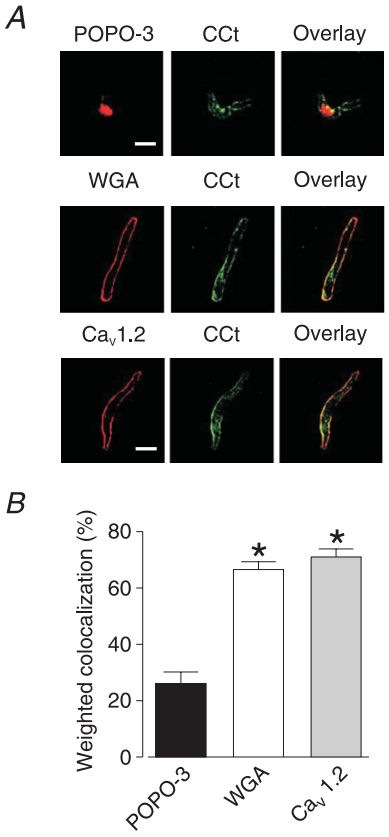

Figure 2. Endogenous CCt locates to the nucleus and plasma membrane in cerebral artery smooth muscle cells
A, representative confocal images illustrating co-localization of endogenous CCt with the nucleus (POPO-3), plasma membrane (WGA) and a commercial $Ca_V1.2$ antibody in isolated arterial smooth muscle cells. Scale bars represent 10 μm. *B*, mean data illustrating weighted co-localization between endogenous CCt, nucleus, WGA or commercial $Ca_V1.2$ antibody. *Significant difference from nuclear co-localization ($P < 0.05$, $n = 6$–7).

channels also locate to the plasma membrane (Fig. 2*A* and *B*).

The anti-CCt antibody recognizes both full-length $Ca_V1.2$ and CCt. To further investigate CCt cellular distribution, GFP-tagged CCt (CCt-GFP) was expressed in cerebral artery smooth muscle cells. CCt-GFP fluorescence co-localized with POPO-3 (~55%), indicating nuclear localization (Fig. 3*A* and *B*). CCt-GFP also co-localized with $Ca_V1.2$ (~37%, Fig. 3*A* and *B*), further suggesting localization with $Ca_V1.2$ channels. A GFP-tagged truncated CCt fragment lacking the nuclear translocation sequence (Δ92CCt-GFP) did not locate to the nucleus, but co-localized with $Ca_V1.2$ (~69%, Fig. 3*C* and *D*) in arterial smooth muscle cells. These data indicate that the CCt fragment locates to both the nucleus and plasma membrane in arterial smooth muscle cells. These data also suggest that CCt can re-associate with, or nearby, short plasma membrane $Ca_V1.2$ channels.

CCt acts as a nuclear-targeting $Ca_V1.2$ transcriptional regulator

Transcriptional regulation by the CCt fragment was investigated in arterial smooth muscle cells. Quantitative real-time PCR was performed on arteries transfected with vectors encoding CCt or Δ92CCt, using empty vector as a control. CCt expression decreased $Ca_V1.2$ mRNA to ~75% of that in control arteries (Fig. 4*A*). In contrast, Δ92CCt expression did not alter $Ca_V1.2$ mRNA (~102% of control, Fig. 4*A*). Rps5 mRNA, the reporter gene used in this assay, was unchanged by expression of either full-length CCt or Δ92CCt (99 ± 3% of control for CCt and 96 ± 1% of control for Δ92CCt).

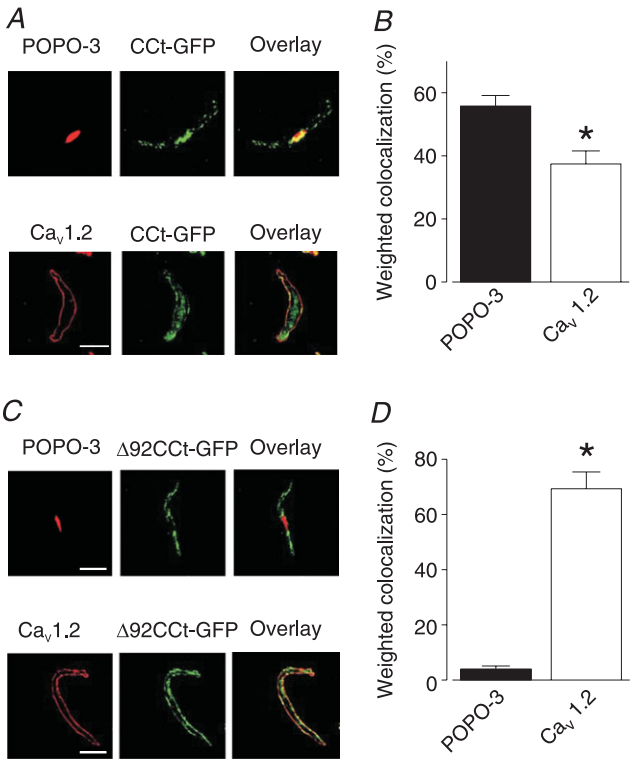

Figure 3. CCt-GFP distributes to the nucleus and plasma membrane in cerebral artery smooth muscle cells
A, representative confocal images illustrating co-localization of GFP-tagged CCt (CCt-GFP) with the nucleus (POPO-3) and a commercial $Ca_V1.2$ antibody in isolated arterial smooth muscle cells. *B*, mean data showing weighted co-localization between CCt-GFP and nucleus (POPO-3) or $Ca_V1.2$. *C*, confocal images illustrating co-localization of GFP-tagged Δ92CCt (Δ92CCt-GFP) with the nucleus or $Ca_V1.2$. *D*, mean data illustrating weighted co-localization between Δ92CCt-GFP and nucleus or $Ca_V1.2$. *Significant difference from nuclear co-localization ($P < 0.05$, $n = 6$–9). Scale bars represent 10 μm.

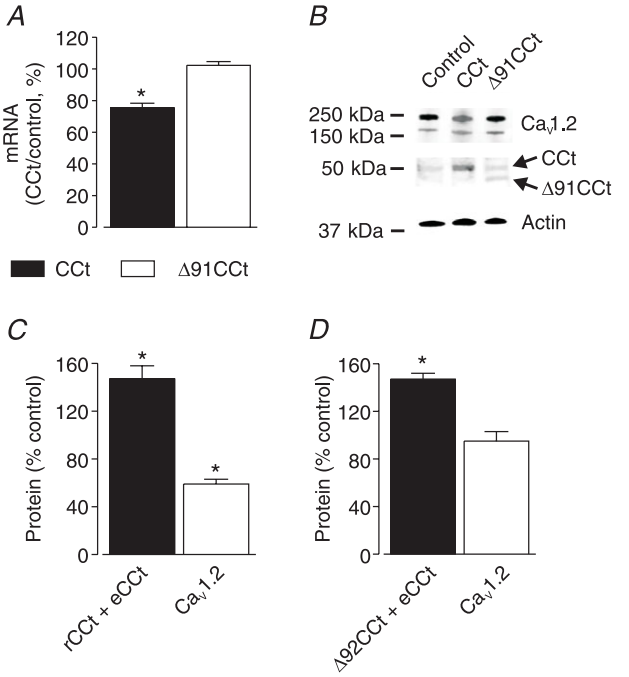

Figure 4. CCt inhibits $Ca_V1.2$ expression in cerebral arteries
A, bar graph illustrating mean $Ca_V1.2$ mRNA transcript levels in cerebral expressing either CCt or Δ92CCt when compared to control. *Significant difference from control ($P < 0.05$, $n = 5$). *B*, representative Western blots illustrating expression of CCt and Δ92CCt and subsequent changes in $Ca_V1.2$ protein in arteries. Blots were cut at the 75 kDa marker. The lower blot was probed for actin and CCt. The upper blot was probed for CCt then stripped and re-probed for $Ca_V1.2$ protein. Brightness and contrast were equally adjusted in all panels to make regions of interest in images clearer. *C*, mean data showing percentage change in total protein for CCt (endogenous, eCCt and recombinant full-length, rCCt) and $Ca_V1.2$ in rCCt-expressing cerebral arteries compared to control. *D*, mean data showing percentage change in total protein for CCt (eCCt and Δ92CCt) and $Ca_V1.2$ in Δ92CCt-expressing cerebral arteries compared to control. *Significant difference from control ($P < 0.05$, $n = 4$–7).

Western blotting indicated that CCt or Δ92CCt expression similarly increased levels of total CCt protein in arteries (Fig. 4*B–D*). CCt expression increased total CCt (endogenous + recombinant CCt) to ∼147% of control (endogenous CCt alone, Fig. 4*B* and *C*). Δ92CCt expression similarly increased total CCt protein (endogenous + recombinant Δ92CCt) to ∼147% of control (Fig. 4*B* and *D*). Probing blots using the anti-CCt antibody demonstrated that CCt expression reduced full-length (240 kDa) $Ca_V1.2$ protein to ∼66% of control (Fig. 4*B* and *C*). Western blotting using the commercial anti-$Ca_V1.2$ antibody indicated that CCt expression reduced total $Ca_V1.2$ (240 kDa and 190 kDa) protein to ∼59% of control (Fig. 4*B* and *C*). In contrast, Δ92CCt did not alter full-length (∼96% of control) or total (∼95% of control) $Ca_V1.2$ protein (Fig. 4*A–D*). CCt or Δ92CCt expression also did not alter the ratio of full-length to short $Ca_V1.2$ protein (1.8 ± 0.3 and 1.6 ± 0.1, respectively), compared to control (1.7 ± 0.3). Taken together, these data indicate that nuclear localization of the CCt fragment inhibits $Ca_V1.2$ gene expression.

CCt reduces $Ca_V1.2$ current density and shifts voltage dependence in arterial smooth muscle cells

Smooth muscle cells were isolated from arteries expressing CCt or Δ92CCt and used for electrophysiology. Ba^{2+} (20 mM) was used as the charge carrier to record $Ca_V1.2$ currents. CCt expression reduced $Ca_V1.2$ current density from ∼2.2 pA pF^{-1} in control to 1.3 pA pF^{-1}, or by ∼42%. CCt also shifted $Ca_V1.2$ current peak voltage from ∼16.8 to 20.6 mV, or by ∼4.8 mV (Fig. 5*A* and *B* and Table 1). CCt shifted the voltage of half-maximal activation ($V_{\frac{1}{2}act}$) from ∼+4.7 to +13.6 mV, or by ∼8.9 mV (Fig. 5*C* and Table 1). The voltage of half-maximal inactivation ($V_{\frac{1}{2}inact}$) was also shifted from ∼−22.3 to −11.5 mV, or by ∼10.8 mV (Fig. 5*D* and Table 1). Non-inactivating $Ca_V1.2$ current decreased from ∼12% of total current in control to 3% in CCt-expressing cells (Fig. 5*D*). CCt expression did not significantly alter the slope of either the steady-state activation or inactivation curves. CCt expression also slowed the rate of current inactivation ∼1.9-fold when compared with control (Fig. 5*E*). Figure 5*F* illustrates

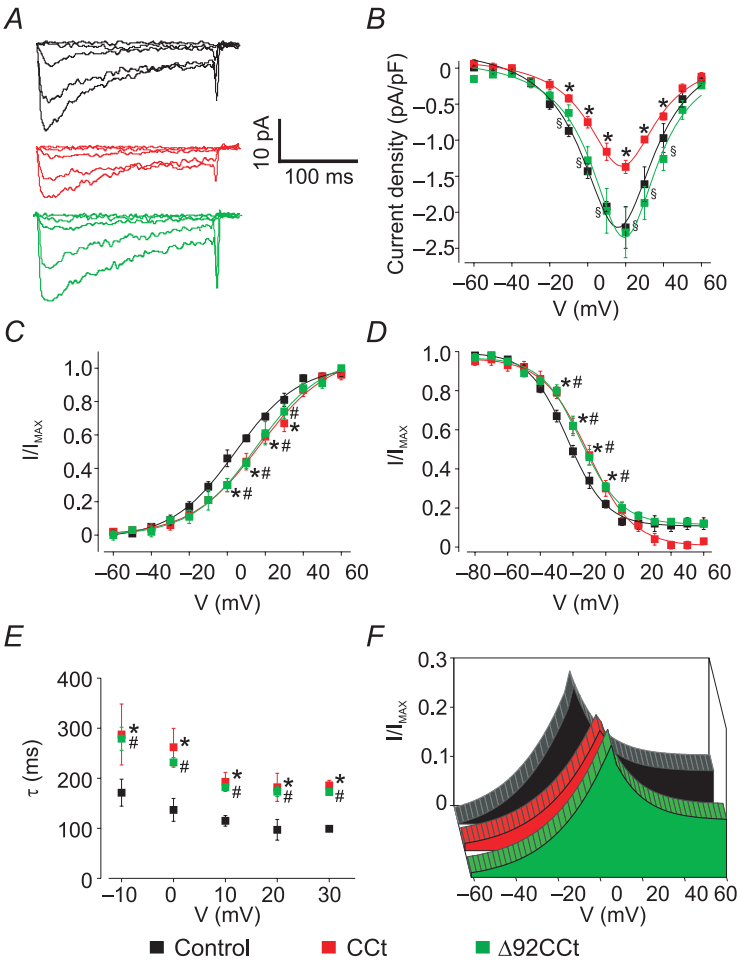

Figure 5. CCt reduces $Ca_V1.2$ current density and shifts voltage dependence
A, representative $Ca_V1.2$ current recordings from control smooth muscle cells and cells expressing CCt or Δ92CCt. For clarity, only steps to −60, −20, 0, +20 and +60 mV are shown. *B*, mean *I–V* relationships of control cells ($n = 10$) and CCt- ($n = 12$) and Δ92CCt-expressing ($n = 8$) arterial smooth muscle cells. *C*, voltage-dependent current activation for $Ca_V1.2$ currents obtained from control cells ($n = 10$) and CCt- ($n = 7$) and Δ92CCt-expressing ($n = 5$) cells. *D*, voltage-dependent current inactivation for $Ca_V1.2$ currents from control cells ($n = 14$) and CCt- ($n = 8$), and Δ92CCt-expressing ($n = 8$) cells. *E*, kinetics of inactivation for control cells ($n = 14$) and CCt- ($n = 8$), and Δ92CCt-expressing ($n = 8$) cells. *F*, plots showing the area under the steady-state activation and inactivation curves (window current) for control cells and CCt- and Δ92CCt-expressing cells. *Significant difference between control and CCt ($P < 0.05$). #Significant difference between control and Δ92CCt ($P < 0.05$). §Significant difference between CCt and Δ92CCt ($P < 0.05$).

Table 1. Properties of $Ca_V1.2$ currents from isolated control cells or cells expressing CCt- or Δ92CCt

	Control	CCt	Δ92CCt
I–V relationship			
Peak current density (pA pF^{-1})	2.2 ± 0.2(10)	1.3 ± 0.1(12)*	2.1 ± 0.3(10)#
Peak voltage (mV)	16.8 ± 0.9(10)	20.6 ± 0.9(12)*	15.5 ± 1.7(10)#
Voltage-dependent activation			
$V_{\frac{1}{2}act}$ (mV)	4.7 ± 0.8(10)	13.6 ± 3.6(7)*	10.3 ± 2.5(5)*
Slope	17.2 ± 1.7(10)	18.1 ± 2.7(7)	15.0 ± 2.3(5)*
Voltage-dependent inactivation			
$V_{\frac{1}{2}inact}$ (mV)	−22.3 ± 1.1(14)	−11.5 ± 1.4(8)*	−15.1 ± 1.8(8)*
Slope	11.0 ± 1.0(14)	12.8 ± 1.3(8)	13.1 ± 1.5(8)

Numbers in parenthesis indicate experimental number. *$P < 0.05$ when compared to control; #$P < 0.05$ when compared to CCt.

effects of CCt expression on arterial smooth muscle cell $Ca_V1.2$ window currents.

The CCt fragment can re-associate with short $Ca_V1.2$ subunits via a proline rich domain (Gerhardstein *et al.* 2000), which is present in the Δ92CCt construct used here. Δ92CCt expression did not alter $Ca_V1.2$ current density (2.3 ± 0.3 pA pF^{-1}), but shifted peak voltage, the $V_{\frac{1}{2}act}$ and the $V_{\frac{1}{2}inact}$ (~5.3 and ~7.2 mV, respectively) similarly to CCt (Fig. 5*A* and *B* and Table 1). Δ92CCt also shifted the voltage dependence of the window current and slowed inactivation kinetics ~1.7-fold (Fig. 5*C–F*). These data suggest that CCt reduces $Ca_V1.2$ current in arterial smooth muscle cells through two different mechanisms: transcriptional inhibition of $Ca_V1.2$ channels reduces $Ca_V1.2$ current density, and re-association with short $Ca_V1.2$ channels right shifts voltage-dependent activation.

CCt dilates cerebral arteries

To examine the functional significance of CCt in arterial smooth muscle cells, pressure-induced vasoconstriction (myogenic tone) was measured in small (~250 μm diameter) cerebral arteries in which recombinant CCt or Δ92CCt were expressed. An elevation in intravascular pressure to 20 or 60 mmHg in control (empty vector) arteries stimulated the development of ~11% and 25% myogenic tone, respectively (Fig. 6*A* and *B*). Membrane depolarization (60 mM K^+, 60 mmHg) constricted control arteries to ~54% of passive diameter (Fig. 6*C*). CCt expression reduced myogenic tone by ~42 and 45% at 20 and 60 mmHg, respectively (Fig. 6*A* and *B*). CCt also reduced depolarization-induced vasoconstriction by ~47% (Fig. 6*C*). Δ92CCt reduced myogenic tone at 20 and 60 mmHg by ~25 and 23%, respectively and 60 mM K^+-induced tone by ~38% (Fig. 6*A–C*). Thus, Δ92CCt expression reduced pressure- and depolarization-induced constriction less effectively than CCt. Collectively, these data indicate that CCt dilates cerebral arteries both by reducing $Ca_V1.2$ current density through a transcriptional mechanism and by directly inhibiting $Ca_V1.2$ channels.

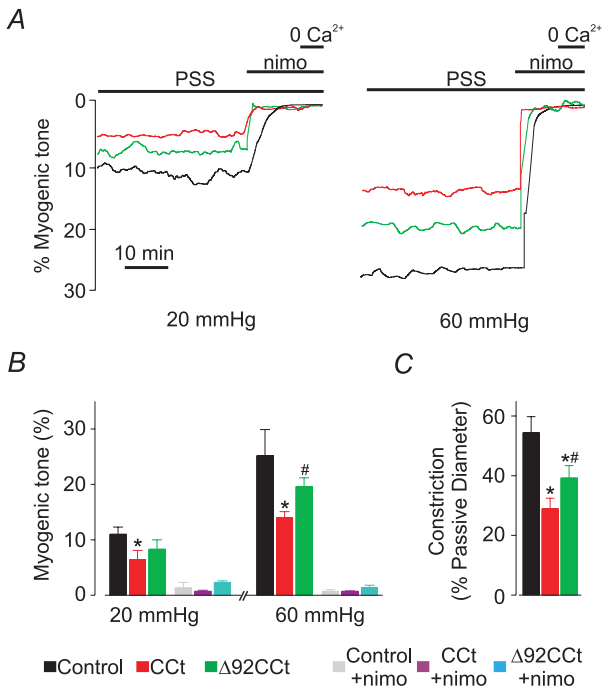

Figure 6. CCt expression reduces pressure- and depolarization induced vasoconstriction in cerebral arteries
A, representative diameter traces illustrating steady-state myogenic tone at 20 and 60 mmHg for control arteries and arteries expressing either CCt or Δ92CCt. *B*, mean data illustrating pressure-induced tone at 20 and 60 mmHg for control and CCt- and Δ92CCt-expressing arteries. *C*, bar graph indicating mean depolarization-induced constriction induced by elevating extracellular K^+ from 6 to 60 mM in control and arteries expressing either CCt or Δ92CCt. *Significant difference between control and CCt ($P < 0.05$). #Significant difference between CCt and Δ92CCt ($P < 0.05$).

Discussion

$Ca_V1.2$ channels are the major Ca^{2+} entry pathway in arterial smooth muscle cells. The existence and physiological functions of the CCt fragment have not been demonstrated in vascular smooth muscle. This study shows for the first time that the CCt fragment is present in smooth muscle cells of small resistance-size arteries. CCt can translocate to the nucleus, leading to a reduction in $Ca_V1.2$ transcription, protein and currents in arterial smooth muscle cells. Data here show that CCt shifts current $V_{\frac{1}{2}act}$, $V_{\frac{1}{2}inact}$, and rate of inactivation, an effect that may be due to re-association with plasma membrane short $Ca_V1.2$ channels. Deletion of the CCt nuclear localization signal abolishes transcriptional inhibition of $Ca_V1.2$, but does not alter modulation of $Ca_V1.2$ current biophysical properties. These data indicate that CCt inhibits $Ca_V1.2$ channel transcription and directly reduces voltage-dependent current activation to inhibit myogenic tone in pressurized arteries. In summary, data show that the CCt fragment is both a bi-modal $Ca_V1.2$ channel inhibitor and vasodilator.

Full length $Ca_V1.2$ subunits are susceptible to post-translational modification by proteolytic processing of their C-terminus to yield a truncated $Ca_V1.2$ channel and a CCt fragment (De Jongh *et al.* 1996). Neuronal and skeletal muscle L-type Ca^{2+} channels are cleaved by calpain, a calcium-dependent cysteine protease (De Jongh *et al.* 1994; Hell *et al.* 1996). Recombinant cardiac $Ca_V1.2$ channels expressed in Sf9 cells are cleaved by chymotrypsin (Gerhardstein *et al.* 2000). In contrast, recombinant $Ca_V1.2$ subunits expressed in Sf9 or HEK cells do not undergo proteolytic cleavage (Chien *et al.* 1995; Puri *et al.* 1997). We and others have previously reported that $Ca_V1.2$ subunits exist as both full length (~240 kDa) and short (~190 kDa) forms in arterial smooth muscle cells (Sonkusare *et al.* 2006; Cheng *et al.* 2007; Xue *et al.* 2007; Bannister *et al.* 2009, 2011). Future studies should aim to determine enzymes responsible for $Ca_V1.2$ cleavage in arterial smooth muscle cells and investigate if this process is regulated physiologically. Such knowledge may demonstrate that control of $Ca_V1.2$ cleavage and CCt production are functional mechanisms to modulate $Ca_V1.2$ currents and vascular contractility. One approach that could have been applied in this study would have been to manipulate endogenous levels of CCt. However, given that mechanisms modulating CCt cleavage are currently unidentified, we overexpressed CCt to study its physiological functions in smooth muscle cells of small resistance-size cerebral arteries.

We previously cloned $Ca_V1.2$ channels ($Ca_V1.2e1b$ and $Ca_V1.2e1c$) expressed in resistance-size cerebral arteries (Cheng *et al.* 2007), the preparation studied here. The amino acid sequences located downstream of the identified cleavage site in $Ca_V1.2$ are identical in $Ca_V1.2e1b$ and $Ca_V1.2e1c$. The predicted molecular weight of both the endogenous and recombinant CCt is ~41 kDa. Our custom anti-CCt antibody detected a similar size band just below the 50 kDa marker in Fig. 1*C* (endogenous) and *A* (overexpressed in HEK cells) and Fig. 3*B* (overexpressed in cerebral arteries). In contrast, Schroder *et al.* (2009) detected a band for CCt at ~37 kDa. It is unknown whether post-translational modification of CCt occurs, or differs in HEK-293, tsA-201 cells, adult ventricular myocytes and arterial smooth muscle cells. Such modifications may explain differences in these apparent molecular weights.

CCt can localize to both the nucleus and plasma membrane in cardiac myocytes and neurons (Gomez-Ospina *et al.* 2006; Schroder *et al.* 2009). Here, we show that both endogenous and recombinant CCt locate to the nucleus and plasma membrane in arterial smooth muscle cells. Given that CCt does not contain transmembrane domains and that CCt-GFP co-localizes with surface $Ca_V1.2$ channels, these data suggest functional interaction. Deletion of a putative conserved nuclear localization sequence within CCt abolished nuclear localization in arterial smooth muscle cells. This result is similar to that described for recombinant CCt expressed in HEK 293T cells (Gomez-Ospina *et al.* 2006). In contrast, deletion of the putative nuclear localization sequence increased nuclear CCt in murine cardiac myocytes (Schroder *et al.* 2009). These data suggest that mechanisms targeting CCt to the nucleus vary in different cell types, but that the previously described nuclear localization sequence is essential for this mechanism in arterial smooth muscle cells. CCt can re-associate with short $Ca_V1.2$ channels via a proline rich domain or via electrostatic interactions between negatively charged glutamate (2103, 2106) and aspartate (2110) residues within CCt and positively charged arginine residues (1696–1697) within the $Ca_V1.2$ C-terminus (Gerhardstein *et al.* 2000; Hulme *et al.* 2006). Here, we used Δ92CCt-GFP, which contains residues necessary for $Ca_V1.2$ re-association, but lacks the proximal 92 amino acids containing the conserved nuclear localization sequence. Δ92CCt-GFP co-localized with plasma membrane $Ca_V1.2$ channels, but was not observed in the nucleus in cerebral artery smooth muscle cells. Imaging data suggest CCt locates to other intracellular localizations that may include endoplasmic reticulum, Golgi and trafficking vesicles. Labelling using the CCt antibody cannot differentiate between the endogenous CCt fragment or full-length $Ca_V1.2$ protein. Therefore, it is not clear if one or both of these proteins locate to other intracellular organelles. In summary, our data suggest that the nuclear localization sequence is essential for CCt nuclear translocation and that CCt re-associates with short $Ca_V1.2$ channels in cerebral artery smooth muscle cells.

$Ca_V1.2$ channel expression is controlled by distinct promoters (Dai *et al.* 2002; Saada *et al.* 2005; Bannister *et al.*

2011). Arterial myocyte $Ca_V1.2$ channels primarily contain exon 1c-encoded N-termini ($Ca_V1.2e1c$), whereas cardiac myocyte $Ca_V1.2$ channels contain N-termini encoded by exon-1b (Blumenstein *et al.* 2002; Liao *et al.* 2005; Cheng *et al.* 2007; Bannister *et al.* 2011). In rat cardiac myocytes, both full-length and truncated CCt reduced $Ca_V1.2$ promoter activity, with truncated CCt inhibiting more than full-length CCt, suggesting increased promoter binding (Schroder *et al.* 2009). In contrast, CCt expression upregulated 66 mRNAs and repressed ∼206 genes in Neuro2A cells in a study in which $Ca_V1.2$ was not identified as a gene altered by CCt (Gomez-Ospina *et al.* 2006). Mice ($DCT^{-/-}$) that express $Ca_V1.2$ channels with a truncation at G1796, which is located in the distal C-terminus, died from congestive heart failure as early as embryonic day 15 (Fu *et al.* 2011). In these mice, cardiac myocyte $Ca_V1.2$ mRNA was similar, whereas $Ca_V1.2$ protein and currents were reduced (Fu *et al.* 2011). Here, CCt expression reduced $Ca_V1.2$ mRNA, $Ca_V1.2$ protein and $Ca_V1.2$ currents in arterial smooth muscle cells. Explanations for this disparity in results are that CCt deletion in cardiac myocytes of $DCT^{-/-}$ mice stimulates $Ca_V1.2$ degradation, or that CCt expression reduces $Ca_V1.2$ mRNA stability. Promoters that control $Ca_V1.2$ expression in arterial smooth muscle cells are poorly understood, with the promoter for $Ca_V1.2e1c$ not reported. Therefore investigating the mechanism of direct regulation of $Ca_V1.2$ promoter activity by CCt in small cerebral arteries is beyond the scope of this project. Taken together, our data suggest that CCt reduces $Ca_V1.2$ transcription, leading to a reduction in protein and current density in arterial smooth muscle cells.

CCt fragment expression reduced peak $Ca_V1.2$ current density and caused a positive shift in $Ca_V1.2$ current $V_{\frac{1}{2}act}$ that would reduce functional voltage-dependent activation in arterial smooth muscle cells. When combined with imaging data in this study and previous data (Gomez-Ospina *et al.* 2006; Hulme *et al.* 2006; Fuller *et al.* 2010), results suggest that CCt re-associates with short $Ca_V1.2$ channels to alter voltage dependence. Consistent with this conclusion, $Ca_V1.2$ currents in cardiac myocytes of $DCT^{-/-}$ mice display a hyperpolarizing shift in $V_{\frac{1}{2}act}$ and increased whole cells currents (Fu *et al.* 2011). CCt expression (residues 1821–2171) reduced recombinant $Ca_V1.2\Delta1821$ current amplitude and shifted the $V_{\frac{1}{2}act}$ to more depolarized potentials in tsA-201 cells (Hulme *et al.* 2006). In a similar study DCT expression reduced recombinant $Ca_V1.2\Delta1800$ current amplitude in a dose-dependent manner in tsA-201 cells (Fuller *et al.* 2010). CCt expression also positively shifted the $V_{\frac{1}{2}inact}$ and slowed current inactivation in arterial smooth muscle cells. In contrast, deletion of the distal C-terminus did not alter the $V_{\frac{1}{2}inact}$ of $Ca_V1.2$ channels or current inactivation in cardiac myocytes of $DCT^{-/-}$ mice (Hulme *et al.* 2006; Fu *et al.* 2011). One explanation for these differences is that mechanisms by which CCt regulates cardiac and smooth muscle cell $Ca_V1.2$ channels may differ. The C-terminus of Ca_V1 channels is encoded by multiple exons, with alternative splicing between exons 40 and 43 occurring in cardiac myocytes (Klockner *et al.* 1997; Soldatov *et al.* 1997; Safa *et al.* 2001; Jurkat-Rott & Lehmann-Horn, 2004). The $Ca_V1.2$ channel C-terminus does not undergo alternate splicing in cerebral artery smooth muscle cells (Cheng *et al.* 2009). Deletion of a proline rich domain within CCt impaired membrane association (Gerhardstein *et al.* 2000). Here, Δ92CCt, in which the nuclear localization sequence is omitted but the proline rich region is retained (Gerhardstein *et al.* 2000), did not alter $Ca_V1.2$ protein or peak $Ca_V1.2$ current density, but shifted $V_{\frac{1}{2}act}$ and $V_{\frac{1}{2}inact}$ similarly to full-length CCt. A recent study demonstrated that Ca^{2+}–calmodulin attenuates $Ca_V1.2$ current inhibition by CCt in HEK293 cells and cardiomyocytes (Crump *et al.* 2013). Here, Ba^{2+} was the charge carrier in patch-clamp experiments. We show in functional experiments that CCt attenuates arterial contractility when Ca^{2+} is the permeant ion. Therefore, these data support the conclusion that CCt inhibits $Ca_V1.2$ when Ca^{2+} is permeant. Future studies should aim to investigate whether Ca^{2+} modifies CCt-regulation of $Ca_V1.2$ currents in arterial myocytes, as is observed in cardiac myocytes (Crump *et al.* 2013). In summary, our data suggest that the CCt fragment can re-associate with short $Ca_V1.2$ subunits, leading to modulation of voltage dependence that reduces channel activity at steady-state physiological potentials in arterial smooth muscle cells.

Elevating intravascular pressure induces steady-state depolarization of smooth muscle cells within resistance-size cerebral arteries to between −60 and −30 mV, with a voltage of ∼−40 mV at a physiological pressure of ∼60 mmHg (Knot & Nelson, 1998). Although CCt and Δ92CCt expression both inhibited pressure- and depolarization-induced vasoconstriction, CCt dilated more so than did Δ92CCt. These data are consistent with CCt decreasing both $Ca_V1.2$ current density and voltage sensitivity, whereas Δ92CCt reduces only $Ca_V1.2$ channel voltage sensitivity. The depolarizing shift in $V_{\frac{1}{2}inact}$ and slower inactivation kinetics caused by both CCt and Δ92CCt overexpression would be expected to prolong $Ca_V1.2$ channel opening and thereby increase Ca^{2+} influx and pressure- and depolarization-induced vasoconstriction. However, the $Ca_V1.2$ window current, a measure of current over a steady-state voltage range, was right shifted. Thus, voltage-dependent activation, which is necessary to induce $Ca_V1.2$-dependent Ca^{2+} influx, is a major factor critical for CCt functionality. These data suggest that CCt attenuates both pressure- and depolarization-induced vasoconstriction by reducing

$Ca_V1.2$ current density and by shifting the $V_{\frac{1}{2}act}$ to more depolarized potentials.

In summary, we demonstrate that the CCt fragment dilates resistance-size cerebral arteries by decreasing $Ca_V1.2$ transcription, protein, and $Ca_V1.2$ channel voltage-sensitivity in smooth muscle cells. These data are consistent with CCt acting as a bi-modal vasodilator.

References

Adebiyi A, McNally EM & Jaggar JH (2008). Sulfonylurea receptor-dependent and -independent pathways mediate vasodilation induced by K_{ATP} channel openers. *Mol Pharmacol* **74**, 736–743.

Amberg GC, Rossow CF, Navedo MF & Santana LF (2004). NFATc3 regulates Kv2.1 expression in arterial smooth muscle. *J Biol Chem* **279**, 47326–47334.

Bannister JP, Adebiyi A, Zhao G, Narayanan D, Thomas CM, Feng JY & Jaggar JH (2009). Smooth muscle cell $\alpha_2\delta$-1 subunits are essential for vasoregulation by $Ca_V1.2$ channels. *Circ Res* **105**, 948–955.

Bannister JP, Bulley S, Narayanan D, Thomas-Gatewood C, Luzny P, Pachuau J & Jaggar JH (2012). Transcriptional upregulation of $\alpha_2\delta$-1 elevates arterial smooth muscle cell voltage-dependent Ca^{2+} channel surface expression and cerebrovascular constriction in genetic hypertension. *Hypertension* **60**, 1006–1015.

Bannister JP, Thomas-Gatewood CM, Neeb ZP, Adebiyi A, Cheng X & Jaggar JH (2011). $Ca_V1.2$ channel -terminal splice variants modulate functional surface expression in resistance size N artery smooth muscle cells. *J Biol Chem* **286**, 15058–15066.

Berridge MJ (1997). Elementary and global aspects of calcium signalling. *J Physiol* **499**, 290–306.

Blumenstein Y, Kanevsky N, Sahar G, Barzilai R, Ivanina T & Dascal N (2002). A novel long N-terminal isoform of human L-type Ca^{2+} channel is up-regulated by protein kinase C. *J Biol Chem* **277**, 3419–3423.

Cartin L, Lounsbury KM & Nelson MT (2000). Coupling of Ca^{2+} to CREB activation and gene expression in intact cerebral arteries from mouse : roles of ryanodine receptors and voltage-dependent Ca^{2+} channels. *Circ Res* **86**, 760–767.

Catterall WA, Perez-Reyes E, Snutch TP & Striessnig J (2005). International Union of Pharmacology. XLVIII. Nomenclature and structure-function relationships of voltage-gated calcium channels. *Pharmacol Rev* **57**, 411–425.

Cheng X, Liu J, Asuncion-Chin M, Blaskova E, Bannister JP, Dopico AM & Jaggar JH (2007). A novel $Ca_V1.2$ N terminus expressed in smooth muscle cells of resistance size arteries modifies channel regulation by auxiliary subunits. *J Biol Chem* **282**, 29211–29221.

Cheng X, Pachuau J, Blaskova E, Asuncion-Chin M, Liu J, Dopico AM & Jaggar JH (2009). Alternative splicing of $Ca_v1.2$ channel exons in smooth muscle cells of resistance-size arteries generates currents with unique electrophysiological properties. *Am J Physiol Heart Circ Physiol* **297**, H680–H688.

Chien AJ, Zhao X, Shirokov RE, Puri TS, Chang CF, Sun D, Rios E & Hosey MM (1995). Roles of a membrane-localized β subunit in the formation and targeting of functional L-type Ca^{2+} channels. *J Biol Chem* **270**, 30036–30044.

Crump SM, Andres DA, Sievert G & Satin J (2013). The cardiac L-type calcium channel distal carboxy terminus autoinhibition is regulated by calcium. *Am J Physiol Heart Circ Physiol* **304**, H455–H464.

Dai B, Saada N, Echetebu C, Dettbarn C & Palade P (2002). A new promoter for α_{1C} subunit of human L-type cardiac calcium channel $Ca_V1.2$. *Biochem Biophys Res Commun* **296**, 429–433.

De Jongh KS, Colvin AA, Wang KK & Catterall WA (1994). Differential proteolysis of the full-length form of the L-type calcium channel $\alpha1$ subunit by calpain. *J Neurochem* **63**, 1558–1564.

De Jongh KS, Murphy BJ, Colvin AA, Hell JW, Takahashi M & Catterall WA (1996). Specific phosphorylation of a site in the full-length form of the $\alpha1$ subunit of the cardiac L-type calcium channel by adenosine 3′,5′-cyclic monophosphate-dependent protein kinase. *Biochemistry* **35**, 10392–10402.

De Jongh KS, Warner C, Colvin AA & Catterall WA (1991). Characterization of the two size forms of the $\alpha1$ subunit of skeletal muscle L-type calcium channels. *Proc Natl Acad Sci U S A* **88**, 10778–10782.

Fu Y, Westenbroek RE, Yu FH, Clark JP, III, Marshall MR, Scheuer T & Catterall WA (2011). Deletion of the distal C-terminus of $Ca_V1.2$ channel leads to loss of β-adrenergic regulation and heart failure *in vivo*. *J Biol Chem* **286**, 12617–12626.

Fuller MD, Emrick MA, Sadilek M, Scheuer T & Catterall WA (2010). Molecular mechanism of calcium channel regulation in the fight-or-flight response. *Sci Signal* **3**, ra70.

Gao T, Bunemann M, Gerhardstein BL, Ma H & Hosey MM (2000). Role of the C terminus of the α_{1C} ($Ca_V1.2$) subunit in membrane targeting of cardiac L-type calcium channels. *J Biol Chem* **275**, 25436–25444.

Gerhardstein BL, Gao T, Bunemann M, Puri TS, Adair A, Ma H & Hosey MM (2000). Proteolytic processing of the C terminus of the α_{1C} subunit of L-type calcium channels and the role of a proline-rich domain in membrane tethering of proteolytic fragments. *J Biol Chem* **275**, 8556–8563.

Gollasch M & Nelson MT (1997). Voltage-dependent Ca^{2+} channels in arterial smooth muscle cells. *Kidney Blood Press Res* **20**, 355–371.

Gomez-Ospina N, Tsuruta F, Barreto-Chang O, Hu L & Dolmetsch R (2006). The C terminus of the L-type voltage-gated calcium channel $Ca_V1.2$ encodes a transcription factor. *Cell* **127**, 591–606.

Hell JW, Westenbroek RE, Breeze LJ, Wang KK, Chavkin C & Catterall WA (1996). *N*-methyl-D-aspartate receptor-induced proteolytic conversion of postsynaptic class C L-type calcium channels in hippocampal neurons. *Proc Natl Acad Sci U S A* **93**, 3362–3367.

Hulme JT, Yarov-Yarovoy V, Lin TW, Scheuer T & Catterall WA (2006). Autoinhibitory control of the $Ca_V1.2$ channel by its proteolytically processed distal C-terminal domain. *J Physiol* **576**, 87–102.

Jaggar JH (2001). Intravascular pressure regulates local and global Ca^{2+} signaling in cerebral artery smooth muscle cells. *Am J Physiol Cell Physiol* **281**, C439–C448.

Jaggar JH, Porter VA, Lederer WJ & Nelson MT (2000). Calcium sparks in smooth muscle. *Am J Physiol Cell Physiol* **278**, C235–C256.

Jurkat-Rott K & Lehmann-Horn F (2004). The impact of splice isoforms on voltage-gated calcium channel α_1 subunits. *J Physiol* **554**, 609–619.

Klockner U, Mikala G, Eisfeld J, Iles DE, Strobeck M, Mershon JL, Schwartz A & Varadi G (1997). Properties of three COOH-terminal splice variants of a human cardiac L-type Ca^{2+}-channel α1-subunit. *Am J Physiol Heart Circ Physiol* **272**, H1372–H1381.

Knot HJ & Nelson MT (1998). Regulation of arterial diameter and wall $[Ca^{2+}]$ in cerebral arteries of rat by membrane potential and intravascular pressure. *J Physiol* **508**, 199–209.

Lesh RE, Somlyo AP, Owens GK & Somlyo AV (1995). Reversible permeabilization. A novel technique for the intracellular introduction of antisense oligodeoxynucleotides into intact smooth muscle. *Circ Res* **77**, 220–230.

Liao P, Yong TF, Liang MC, Yue DT & Soong TW (2005). Splicing for alternative structures of $Ca_v1.2$ Ca^{2+} channels in cardiac and smooth muscles. *Cardiovasc Res* **68**, 197–203.

Puri TS, Gerhardstein BL, Zhao XL, Ladner MB & Hosey MM (1997). Differential effects of subunit interactions on protein kinase A- and C-mediated phosphorylation of L-type calcium channels. *Biochemistry* **36**, 9605–9615.

Saada NI, Carrillo ED, Dai B, Wang WZ, Dettbarn C, Sanchez J & Palade P (2005). Expression of multiple $Ca_V1.2$ transcripts in rat tissues mediated by different promoters. *Cell Calcium* **37**, 301–309.

Safa P, Boulter J & Hales TG (2001). Functional properties of $Ca_V1.3$ (α_{1D}) L-type Ca^{2+} channel splice variants expressed by rat brain and neuroendocrine GH3 cells. *J Biol Chem* **276**, 38727–38737.

Schroder E, Byse M & Satin J (2009). L-type calcium channel C terminus autoregulates transcription. *Circ Res* **104**, 1373–1381.

Soldatov NM, Zuhlke RD, Bouron A & Reuter H (1997). Molecular structures involved in L-type calcium channel inactivation. Role of the carboxyl-terminal region encoded by exons 40–42 in α_{1C} subunit in the kinetics and Ca^{2+} dependence of inactivation. *J Biol Chem* **272**, 3560–3566.

Sonkusare S, Palade PT, Marsh JD, Telemaque S, Pesic A & Rusch NJ (2006). Vascular calcium channels and high blood pressure: pathophysiology and therapeutic implications. *Vascul Pharmacol* **44**, 131–142.

Wei X, Neely A, Lacerda AE, Olcese R, Stefani E, Perez-Reyes E & Birnbaumer L (1994). Modification of Ca^{2+} channel activity by deletions at the carboxyl terminus of the cardiac α1 subunit. *J Biol Chem* **269**, 1635–1640.

Xue JH, Zhang LF, Ma J & Xie MJ (2007). Differential regulation of L-type Ca^{2+} channels in cerebral and mesenteric arteries after simulated microgravity in rats and its intervention by standing. *Am J Physiol Heart Circ Physiol* **293**, H691–H701.

Additional information

Competing interests

None.

Author contributions

All experiments were performed in the laboratory of Professor Jonathan H. Jaggar in the Department of Physiology at UT-Health Science Centre, Memphis, TN, USA. The authors contributed to the study as follows: J.P.B. contributed significantly to the conception and design of experiments, collection, analysis and interpretation of data and to the drafting of the article or revising it critically for important intellectual content. M.D.L. contributed significantly to the collection, analysis and interpretation of data and to the drafting of the article or revising it critically for important intellectual content. D.N., W.J., A.N., K.W.E., J.P., K.S.G. and F.A.B. contributed significantly to the collection, analysis and interpretation of data. J.H.J. contributed significantly to the conception and design of experiments and to the drafting of the article or revising it critically for important intellectual content. All authors approved the final version of the manuscript.

Funding

This work was supported by grants to J.H.J from NIH/NHLBI.

Acknowledgements

We thank Dr Simon Bulley for critical reading of the manuscript.